Self-diffusion of iron in $L1_0$-ordered FePt thin films

M. Rennhofer, B. Sepiol, M. Sladecek, D. Kmiec, S. Stankov,* and G. Vogl
Institut für Materialphysik der Fakultät für Physik, Universität Wien, Strudlhofgasse 4, A-1090 Wien, Austria

M. Kozlowski and R. Kozubski
M. Smoluchowski Institute of Physics, Jagiellonian University Cracow, Reymonta 4, PL 30-059 Cracow, Poland

A. Vantomme and J. Meersschaut
Instituut voor Kern en Stralingsfysica and INPAC, K. U. Leuven, Celestijnenlaan 200D, B-3001 Leuven, Belgium

R. Rüffer
ESRF, 6 rue Jules Horowitz, Boîte Postale 220 38043 Grenoble Cedex, France

A. Gupta
CSR Indore Centre, Khandwa Road, Indore 452 017, India

(Received 28 February 2006; revised manuscript received 19 May 2006; published 15 September 2006)

Diffusion of iron atoms in a thin FePt film of $L1_0$ structure was investigated in the low temperature region where iron diffusivities are between 10^{-22} m^2 s^{-1} and 10^{-24} m^2 s^{-1}. A new method using nuclear resonant scattering of synchrotron radiation in grazing incidence geometry was used, providing higher accuracy and sensitivity than the conventional tracer methods. Isotopical FePt multilayer samples Pt(20 Å)/[^{57}FePt(20 Å)/FePt(30 Å)]$_{10}$/MgO(001) produced by molecular beam epitaxy were annealed at four temperatures between 773 and 873 K for times between 60 and 120 min. The nuclear reflectivity was measured at room temperature after each annealing step and the decrease of the nuclear superstructure Bragg-peak intensities was observed. From the intensity loss, the diffusion coefficient and the activation energy for iron self-diffusion in the FePt thin film along the c axis were determined as $D_0=(3.45\pm0.44)\times10^{-13}$ m^2 s^{-1} and $Q=(1.65\pm0.29)$ eV. The value for the activation energy is the same as found by residual resistivity measurements in the same system.

DOI: 10.1103/PhysRevB.74.104301 PACS number(s): 66.30.Fq, 61.10.Kw, 61.66.Dk, 68.55.−a

I. INTRODUCTION

While FePt is a main candidate for next generation data storage devices, its physical properties regarding diffusion are nearly unknown. There have been various experiments with bulk FePt (Refs. 1–3) dealing with diffusion and ordering, respectively. No diffusion data except for radio-tracer data and chemical diffusion data in the high-temperature range and in the disordered fcc phase exist.[1,2] In this work we present results on diffusion in $L1_0$-ordered FePt thin films, deposited on MgO(001) substrate, achieved by means of nuclear resonant scattering. For a model of the $L1_0$ structure; see Fig 1. To study the self-diffusion of Fe in FePt thin films with high spatial resolution we used a method[4] exploiting the grazing incidence nuclear resonant scattering (GINRS) of synchrotron radiation.[5–7]

Up to now, the radio-tracer technique has been used to study mesoscopic and macroscopic diffusion dynamics.[8] On the atomic scale, scattering methods as quasielastic Mössbauer spectroscopy, nuclear resonant scattering (NRS), and quasielastic neutron scattering are state of the art in the field.[9,10] The disadvantage of all scattering methods is the very limited range of accessible diffusion coefficients. The main drawback of the radio-tracer method is that it is dealing with radioisotopes and the measurement is destructive. Further, the resolution of diffusion depths is limited by the detector efficiencies and sputtering resolving power. Combining the principles of the two methods, i.e., tracer atoms to investigate the diffusion length of nuclei and nuclear resonant scattering to resolve isotopes, we obtain a powerful tool for studying dynamical processes on the nanometer scale. DuMond and Youtz have shown that it is possible to use x-ray scattering contrast of a deposited multilayer structure of chemically different elements to measure interdiffusion in gold-copper multilayers.[11] Cook and Hillard laid the theoretical background using the method for studying interdiffusion coefficients in gold-silver alloys.[12] The method was used for investigations of diffusion on the nanoscale by x-ray and neutron scattering[13,14] by measurement of superstructure Bragg peaks originating from the modulated layer structures. An intermixing of the modulated structure due to dynamical processes can be related to a decrease of intensity of the

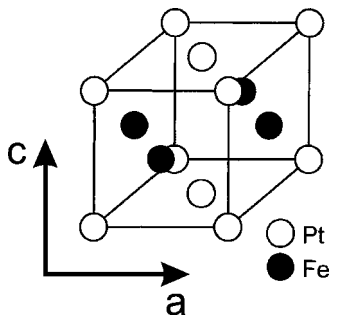

FIG. 1. $L1_0$ structure of FePt with alternating monoatomic planes of Fe and Pt.

superstructure Bragg peaks. In a nuclear resonance experiment the sensitivity is extended from chemically different elements to different isotopes. The use of the Mössbauer isotope ^{57}Fe with its nuclear-resonance transition at 14.4 keV allows us to study diffusion coefficients below 10^{-24} m^2 s^{-1} in chemical equilibrium with high resolution of the diffusion length.[4]

We want to point out that there were also approaches to use isotopic layer structures for diffusion studies, where the layer profile was probed via secondary ion mass spectrometry (SIMS).[15,16] While the experiments gave access to rather low diffusivities, the method was nevertheless destructive.

The FePt alloy form a $L1_0$ phase for a wide range of concentrations around stoichiometry from 33 at % Pt to 55 at % Pt at 873 K. The temperature of the "order-disorder" transition is 1553 K. The $L1_0$ phase has a large magnetocrystalline uniaxial anisotropy in the range between 7 J cm^{-3} (Ref. 17) and 80 J cm^{-3} (Ref. 18) which makes it ferromagnetically stable. The system is a hard magnet with a very high magnetocrystalline anisotropy of 0.5 meV per 3d atom.[19] Therefore, FePt is of high technological interest for applications such as data-storage devices. The magnetocrystalline and thermal stability makes this compound suitable for ultrahigh density recording. A detailed knowledge of the dynamic and diffusion processes is essential for selectively designing alloys with different physical properties for technical applications.

II. SAMPLE PREPARATION

The quality of FePt thin films strongly depends on the modification of the preparation conditions, such as deposition temperature,[20,21] buffer-layer material, and thickness.[21,22] The FePt alloy is of $L1_0$ structure with lattice constants of a=3.8504(8) Å and c=3.7212(3) Å.[23] This gives a lattice misfit on the MgO(001) surface (a_{MgO} =4.21 Å) of 9% but only 1.6% on a Pt buffer (a_{Pt}=3.92 Å).[22,24] Therefore a Pt-buffer layer relaxing the stress of the lattice misfit is usually used when preparing thin FePt films. On the other hand, the use of buffer layers can easily induce growth of $L1_0$-ordered FePt islands, where the height and width of the islands strongly depends on the deposition temperature and buffer-layer thickness.[20,22] To avoid the island growth and to guarantee a flat film, no buffer was used. The stress in the $L1_0$ structure can be reduced only by the formation of microtwins,[22] destroying the perfect single-crystalline order. For the measurement we performed, the loss of the single-crystalline order was of no relevance. The sensitivity of our experiment was only for iron diffusion along the c axis of the FePt sample whereas the microtwins represent different orientated domains along the a axis.

The samples were deposited using molecular beam epitaxy on MgO(001) substrates. The multilayer was nominally prepared as Pt(20 Å)/[^{57}FePt(20 Å)/FePt(30 Å)]$_{10}$/MgO, where the 20-Å-thick ^{57}FePt layers contain only ^{57}Fe, while the 30-Å-thick FePt layers are prepared using iron with natural abundance of ^{57}Fe (2.14%). The FePt layers were deposited at 623 K in a vacuum better than 1.3×10^{-10} mbar. A capping layer of 20 Å Pt, deposited at room temperature,

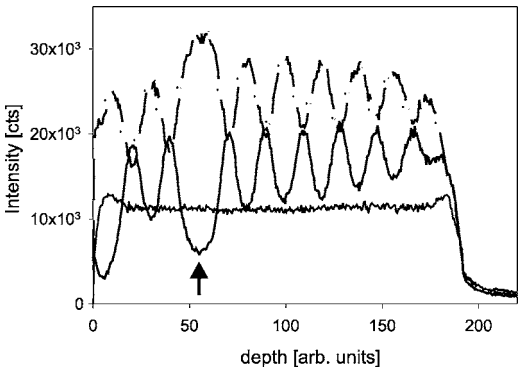

FIG. 2. Secondary ion mass spectrographic depth profile for the FePt multilayer. The solid line shows the concentration of ^{57}Fe, the dotted-dashed line the concentration of ^{56}Fe. The horizontal line shows the Pt concentration. The third ^{57}FePt layer (indicated by the arrow) is missing; instead, FePt with a natural abundance of ^{57}Fe was deposited.

prevented the oxidation of the multilayer. All experiments on thin-film samples reported in this work were performed on parts that were cut from one sample. A moderate deposition temperature was chosen to guarantee a well-ordered $L1_0$ structure[20,21] but, simultaneously, to prevent the isotopic multilayer structure from mixing during the deposition process. Moreover, the low deposition temperature avoids the formation of islands.[20] The composition was checked post-annealed via Rutherford backscattering (RBS) and was $Fe_{50}Pt_{50}$ with an accuracy of 1 at %. Furthermore, the RBS yield is a measure for the crystalline quality (or epitaxy) of the thin film. Its value can range from 100% for a polycrystalline sample to just a few percent in case of perfect epitaxy. The values found for the FePt thin-film samples is 10%. This is a proof that the layer remains uniform after annealing (no islanding), and maintains its good crystalline quality. The isotopic stoichiometry was determined by SIMS, see Fig. 2. The analysis shows a disturbance in the layer periodicity, the third bilayer consisted of natural iron only, indicated by the arrow in Fig. 2. In the nuclear resonant spectra this led to a splitting of the nuclear Bragg peaks, see Fig. 3 and Sec. III B for details.

The crystalline order of the films was checked by x-ray diffraction (XRD), see Fig. 4, and the magnetic order by NRS in the time domain, see Fig. 5. In Fig. 4, the (001), (002), and (003) $L1_0$ peaks of FePt can be seen, indicating the $L1_0$ structure. The c-axis lattice constant of the tetragonal structure, calculated from the position of the peaks, c_{exp} =3.714(7) Å, corresponds with the literature value of the c axis in the $L1_0$ FePt structure c_{id}=3.7212(3) Å.[23,25] The Pt(001) and Pt(002) peaks originate from the 20 Å thick cover layer of pure Pt. The long-range order parameter S (Refs. 23 and 25) for the FePt thin film was calculated from the intensities of the fundamental and superstructure peaks (002) and (003) of the x-ray diffraction spectra. S is 0.77(5) at the preparation temperature at 623 K, and increases to S =0.94(6) at 873 K. The high degree of order results from the elongation of the in-plane axis (a axis) due to the misfit with the substrate and results in the reduction of the out-of-plane axis (c axis) which promotes the formation of the $L1_0$ structure.

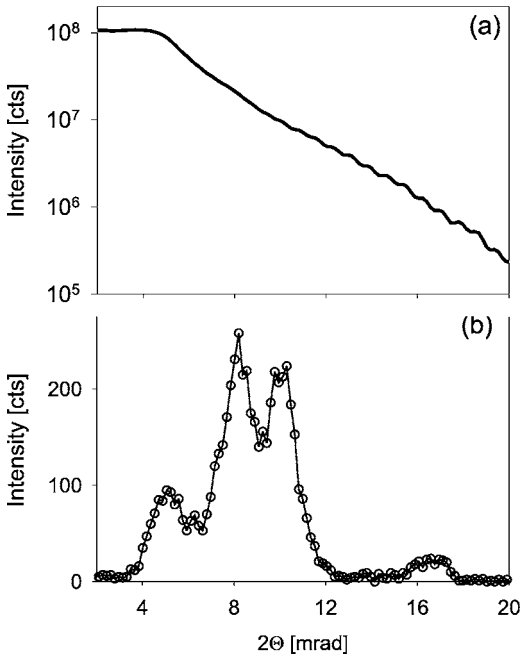

FIG. 3. (a) Electronic reflectivity and (b) nuclear reflectivity of the FePt multilayer as prepared at 623 K. The isotopic bilayer structure is only reproduced in the nuclear reflectivity. At the critical angle [5.15(2) mrad] the nuclear total reflection peak is observed. Due to the layer periodicity the first-order nuclear Bragg peak is split, and results in intensity maxima at 8.12(3) and 10.12(3) mrad. The second-order nuclear Bragg peak is located at 16.58(5) mrad.

The spectra in Fig. 5 show the nuclear resonant scattered intensity in the time domain of the as-prepared FePt thin film. Spectrum (a) was measured with the direction of the wave vector of the incoming photons parallel to the a axis of the FePt $L1_0$ structure; spectrum $5(b)$ was measured after rotating the sample 45 degrees around the c axis. Both spectra were recorded under the grazing incidence angle. They were fitted with the same parameters and confirm that the magnetic field vector is perpendicular to the surface of the thin film. This proves that the samples were c variant, not less than about 98%, i.e., the c axis of the thin film perpendicular to the sample surface.

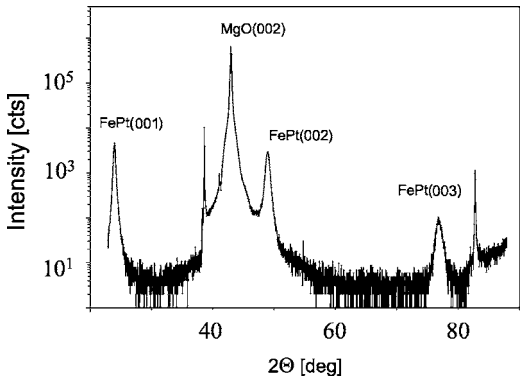

FIG. 4. XRD image of the FePt thin film as prepared at 623 K. The FePt(001), (002), and (003) peaks can be seen.

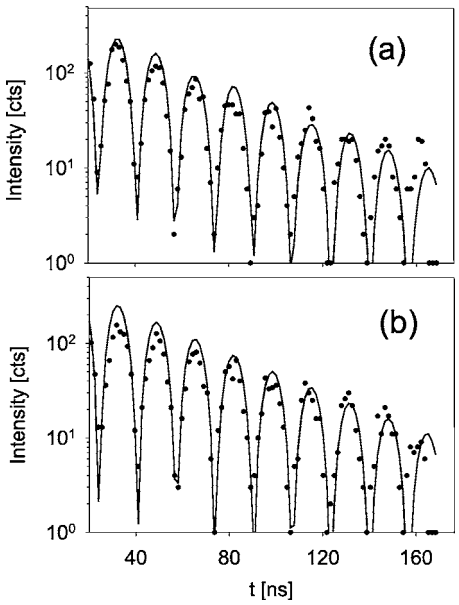

FIG. 5. NRS spectra in the time domain of the FePt thin film as prepared at 623 K. In spectrum (a) the incoming wave vector was oriented parallel to the a axis of the $L1_0$ structure; in spectrum (b) the sample was rotated 45 degrees. The fits in both spectra (solid line) are consistent with the fact that the magnetic field vector $\vec{H}$ is perpendicular to the thin-film surface.

III. NUCLEAR RESONANT SCATTERING

A. Theory

The intensity of x rays reflected from a periodically modulated structure, e.g., from a repeated bilayer structure, shows superstructure peaks at angles corresponding to the layer periodicity. If the bilayer structure is chemically inhomogeneous, i.e., alternating layers are formed of different atoms, the layer periodicity can be detected via the electronic reflectivity and the nuclear resonant reflectivity. When the bilayer is chemically homogeneous, i.e., formed of the same kind of atoms, the electronic reflectivity will show no superstructure peaks, only the thickness oscillations (Kiessig beats) corresponding to the total thickness of the multilayer, see Fig. 3(a). However, the use of different isotopes in alternating layers, e.g., ^{56}Fe and ^{57}Fe, provides the access to the layer structure by the use of nuclear resonant scattering. The intensity of nuclear resonant scattered synchrotron radiation, i.e., the *delayed* intensity, shows *nuclear* Bragg peaks that correspond to the periodicity of alternating isotopic layers; see Fig. 3(b).

The following derivation of the diffusion coefficient combines those of DuMond and Youtz[11] and Cook and Hillard,[12] using up-to-date diction regarding diffusion. Let $\rho_A(x,t)$ and $\rho_B(x,t)$ be the mass of atoms of the species A and B per unit volume of the mixture in an isotopic multilayer at the position x and time t, and V_A and V_B be the volume occupied by atoms of the type A and B per unit mass of the mixture, respectively. Then the mass fraction of atoms of type A and B of the multilayer are $V_i\rho_i(x,t)$ with $i=A,B$, which must be preserved in the multilayer

TABLE I. Parameters for the annealing procedure of the FePt thin films, and diffusion coefficients for the FePt thin-film samples.

	Annealing step (min)				
Sample / T (K)	1	2	3	4	D (10^{-24} m^2 s^{-1})
*P*1/823	60	60	60	60	20±6
*P*2/873	60	60	30	30	101±2
*P*3/773	60	60	120	120	6.9±2.5
*P*4/848	60	60	60	60	76±11

$$V_A\rho_A(x,t) + V_B\rho_B(x,t) = 1. \tag{1}$$

From the definition of $\rho_A(x,t)$ and D being the concentration independent diffusion coefficient, the diffusion equation holds:

$$\frac{\partial\rho_A}{\partial t} = D\frac{\partial^2\rho_A}{\partial x^2}. \tag{2}$$

As $\rho_A(x,t)$ is a periodic function with period L, it can be expanded in a Fourier series with period L and decaying exponentially with time t. For a multilayer structure composed of repeated bilayers, this would be the bilayer periodicity L smeared out after a time t due to diffusion processes. The series can be written as

$$\rho_A(x,t) = \sum_{n=0}^{N}\left[S_n e^{-\sigma_n t}\sin\left(\frac{2\pi nx}{L}\right) + C_n e^{-\gamma_n t}\cos\left(\frac{2\pi nx}{L}\right)\right], \tag{3}$$

where σ_n and γ_n are constants. The series then represents the artificially imposed periodicities. Substituting this into Eq. (2) and comparing the coefficients one gets

$$\sigma_n = \gamma_n = \frac{4\pi^2 n^2}{L^2}D. \tag{4}$$

The density distribution in space decays with time t, i.e., is smeared out, with an exponential dependence exp $[-4D\pi^2n^2t/L^2]$. As the amplitude of the nuclear Bragg peaks is calculated from the layer periodicity, it shows a similar exponential containing the layer periodicity L and the diffusion coefficient D

$$A(t) = A(0)\exp\left[-\frac{4D\pi^2m^2}{L^2}t\right]. \tag{5}$$

Note that here m denotes the order of the nuclear Bragg peak. In the measurement only the intensity I is observed, with $I\sim|A|^2$. Since the intensity of all nuclear Bragg peaks of orders greater than one are very small and decaying much faster, only the nuclear Bragg peak of first order was used for the evaluations (see also Sec. III B). By calculating the logarithmic ratio between the intensity at time t and at time zero, $\ln[I(t)/I(0)]$ for the first-order nuclear Bragg peak ($m=1$), one gets the time dependence of the dynamics in the system. Further, for the time differential, this yields the relation for the determination of D

$$\frac{d}{dt}\ln\left(\frac{I(t)}{I(0)}\right) = -\frac{8\pi^2}{L^2}D. \tag{6}$$

By calculating the logarithmic ratio of the intensities for successive annealing steps, one can determine the diffusion coefficient D for one annealing temperature T. For different annealing temperatures T_i an Arrhenius plot D vs $1/T$ can be obtained. The activation energy Q for the single diffusion jump of the iron atom can be derived via

$$D(T) = D_0\exp\left[-\frac{Q}{k_BT}\right], \tag{7}$$

with k_B the Boltzmann constant and D_0 a material constant.

B. Experiment and results

The nuclear resonant scattering experiments were done at the beamline ID22N of ESRF. The setup is the one for nuclear resonant scattering in grazing incidence geometry (GINRS), see Ref. 5 for details. The samples were annealed stepwise at temperatures of 773, 823, 848, and 873 K for times between 30 and 120 min; see Table I.

The annealing was accomplished in a quartz tube furnace in a vacuum of 10^{-6} mbar. The insertion and removal of the samples from the heating zone in a low-heat capacity sliding shuttle was fast to assure a cooling down by thermal radiation within 30 s to temperatures below 400 K, still in the vacuum. The fast heating and cooling enabled a well-defined annealing time. The GINRS measurements were performed in air at room temperature. Θ-2Θ scans were taken for the first two orders of nuclear Bragg peaks of the multilayer structure (as shown in Fig. 3). The delayed nuclear scattered intensity and the prompt electronic reflectivity were measured simultaneously between 10 and 50 s per point for a scan. The data were normalized for the synchrotron-beam intensity. The small-angle x-ray scattering background with its q^{-4} angular dependence was found to be negligibly small and was therefore not taken into account.

The performed experiment gives exclusive access to diffusion of iron along the c axis of the FePt $L1_0$ structure. This results from the geometry of the GINRS setup and the orientation of the isotopic multilayer structure. The scattering vector and the c axis of the FePt thin film were both perpendicular to the sample surface.

As self-diffusion of iron atoms occurs during the annealing for a defined time at temperature T, the isotopic bilayer

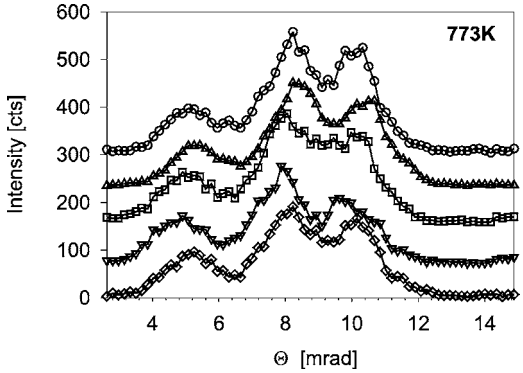

FIG. 6. Nuclear Bragg peaks for the FePt thin film after stepwise annealing at 773 K, as prepared (○), after 60 (△), 120 (□), 240 (▽), and 360 min (◇). The lines are guides for the eyes, and the spectra are shifted by 75 counts relatively to each other for clarity.

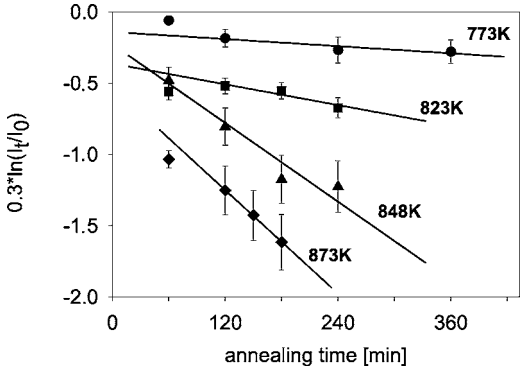

FIG. 7. Logarithmic ratio $\ln[I_t/I_0]$ of the Bragg-peak intensities versus the total annealing time at 773 (●), 823 (■), 848 (▲), and 873 K (◆). The lines are linear regressions. The slopes correspond to the diffusion coefficients.

structure is smeared out. Consequently, the spectra show a decrease of the nuclear Bragg-peak intensity.

The spectra of electronic and nuclear reflectivity for the as-prepared sample are shown in Fig. 3(a) and 3(b), respectively. The electronic reflectivity shows a beat pattern corresponding to the total film thickness. The angle of the total reflection is $\Theta_C=5.15(2)$ mrad. The nuclear Bragg peaks can be seen at angular positions corresponding to the bilayer period. The peak at the lowest angle corresponds with the total reflection angle of the synchrotron radiation on a FePt layer covered by Pt.[6] The double-peak structure of the nuclear Bragg peak which is visible for the first-order Bragg peak at 8.12(3) and 10.12(3) mrad is due to the disturbance in the bilayer periodicity, as was discussed in Sec. II. The second-order Bragg peak at a position of 16.58(5) mrad is of low intensity, which makes the calculation of diffusion using the second-order Bragg peaks impossible.

Exemplary spectra after successive annealing steps at 773 K are shown in Fig. 6. The position of the total reflection peak remains the same for all annealing steps. This indicates that the chemical composition of the sample did not change significantly during the annealing. The first-order nuclear Bragg peaks were fitted by a sum of two Gaussians. The diffusion coefficients $D(T)$ at 773, 823, 848, and 873 K were calculated from the intensity loss of the nuclear Bragg peaks via Eq. (6). The logarithmic ratio of the peak intensities versus total annealing time is presented in Fig. 7 [more precisely $L^2 \ln(I_T/I_0)/8\pi^2$ is plotted vs Dt]. The slope of the exponential function is the diffusion coefficient $D(T)$ for the annealing temperature T. All calculations were done for the first-order nuclear Bragg peaks. For the weighted regression curves the first point of each time series was not taken into account due to relaxation effects in the thin film during the first annealing step; see also Refs. 4 and 13.

The results are summarized in Table I. The diffusion coefficients at all temperatures follow Arrhenius behavior. The plot for the activation energy is shown in Fig. 8 (circles), and is compared to high-temperature radio-tracer data (triangles showing up and down) and interdiffusion data (squares and diamonds) which were measured near the order-disorder transition point. The slope of the Arrhenius plot corresponds to an activation energy of $Q=(1.65\pm0.29)$ eV with the constant $D_0=(3.45\pm0.44)\times10^{-13}$ m^2 s^{-1}.

IV. DISCUSSION AND CONCLUSIONS

Our data from nuclear resonant scattering reveal information about the iron diffusion along the c direction in the thin film. Figure 8 represents the comparison with radio-tracer data[1] of Fe in $Fe_{54}Pt_{46}$ for the high-temperature region close to the point of the order-disorder transition. Chemical diffusion data for diffusion of Fe in $Fe_{55}Pt_{45}$[2] are shown for completeness. All tracer data correspond to iron diffusion in bulk FePt along the a direction and the c direction. For the bulk data one finds a higher activation energy for the diffusion along the c direction than along the a direction. This holds for chemical diffusion and radio-tracer measurements. In the a direction the atoms may diffuse within the iron planes; see Fig. 1. In the c direction the iron atoms have to diffuse through the layers of platinum atoms via antistructure lattice sites. There exists no nearest-neighbor jump vector to iron sites in this direction. The next-nearest-neighbor jumps are

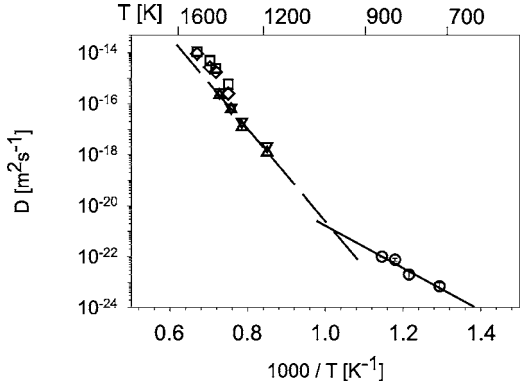

FIG. 8. Arrhenius plot for iron diffusion in FePt. The NRS data for diffusion along the c direction in the thin film are indicated by circles (○), whereas (▽) and (△) are radio-tracer data for iron diffusion in bulk FePt along the a and c directions, respectively (see Ref. 1) Chemical tracer data are shown as (□), a direction, and (◇), c direction, for iron diffusion in bulk FePt (Ref. 2).

energetically less favorable than diffusion along the *a* direction, i.e., in the layers of pure iron. A similar phenomenon has been observed for titanium self-diffusion in γ TiAl (Refs. 26 and 27) and iron diffusion in B20-type FeSi.[28] Nevertheless, the activation energy for diffusion in the low-temperature region of 1.65(29) eV, obtained by the nuclear resonant scattering experiment, is significantly lower than the activation energies from high-temperature radio-tracer data in bulk crystals in directions of the *a* and *c* axes, 3.38(23) eV and 3.59(21) eV, respectively. Also for the preexponential factor D_0 of Eq. (7), the value $3.45(44) \times 10^{-13}$ m^2 s^{-1} is significantly lower than the values which one can estimate from the radio-tracer data for diffusion along the *a* and *c* directions, respectively.

Our results are in agreement with the activation energies for "order-order" relaxations from residual resistivity measurements on $Fe_{50}Pt_{50}$ bulk polycrystalline sample and *in situ* resistivity measurements of the FePt thin film (the same as we used in the NRS experiment). Details about the measurements are published elsewhere.[3] We find an activation energy for order-order relaxations of 1.5(3) eV for the polycrystalline bulk sample and 1.8(2) eV, for the thin film sample at temperatures below about 850 K.[3] Surprisingly we find a higher activation energy of 2.7(1) eV at higher temperatures in the bulk sample and a discontinuous change of the activation energy. The thin film sample was not measured up to this temperature. The activation energy achieved represents the activation energy for migration of Fe in *c*-direction of the film (i.e., change of order due to antisites), as change in resistivity is not sensitive to the migration of iron atoms along the *a* direction (i.e., in the plane of iron no change of order takes place).[29]

The most surprising result of our measurement is the low value of the preexponential factor D_0 and of the activation energy Q. Especially D_0 value is orders of magnitude lower than in pure metals and intermetallic alloys. Only for interdiffusion in bulk diffusion couples[30] a comparable low value for D_0 of $3.45(44) \times 10^{-13}$ m^2 s^{-1} with also lower activation energy than achieved by the radio-tracer technique was found. In the interdiffusion experiment the specimen used were annealed to induce grain growth. The low values for D_0 and Q in Ref. 30 could be interpreted as result of short-circuit diffusion along grain boundaries. In our opinion the low values of D_0 and Q in the thin-film sample are an indication of a highly correlated mechanism of atomic diffusion at low temperatures. This shall be discussed in the following.

It is known from the literature that the stress in thin layers of FePt relaxes via creation of microtwins oriented along the [100] and [010] directions. The thin film stays a single crystal[22] and the twinning causes creation of antiphase boundaries, with low volume fraction as the mean size of the microtwins ranges from 50 to 200 nm.[22] No grain boundaries were observed for the preparations of the thin FePt film directly on the MgO substrate.[22] In our opinion the most important argument for the "bulk" character of diffusion in our experiments is the equivalence of the activation energy achieved by NRS, with that of the order-order relaxation. The discontinuous change of the activation energy observed in Ref. 13 in the bulk sample, staying the same for heating up or cooling down, cannot be explained via a short-circuit diffusion process. Moreover, this effect was so far exclusively observed in the low-temperature region of the FePt $L1_0$ phase and never in any other intermetallic phase, neither single nor polycrystalline. The origin of the discontinuous change is not understood yet.

A significant enhancement of diffusivity with low activation energies was observed in near-surface layers of iron and iron silicide films.[7,31] However, this effect is limited to the upper 3 nm of the sample and in no case can it explain lower activation energy in our 50 nm-thick isotopic multilayer sample.

The exact defect structure, i.e., the amount of antistructure atoms and their species, vacancies and their distributions, etc., of the FePt system in bulk or thin films needs much more investigation. This would allow us to definitely conclude on the mechanisms of diffusion. Therefore, we cannot exclude that there is a contribution to diffusion via low correlated mechanisms as short-circuit or grain-boundary diffusion. Nevertheless, following our argumentation above, we think that the contribution of these mechanisms to the overall diffusion is small. Possible elementary jumps for the $L1_0$ are presented in Ref. 32 for the TiAl alloy. The jump sequences the authors describe there are favorable for low correlated diffusion mechanisms. For finding analogies for the diffusion mechanisms one has to be careful, taking into account that the γ-TiAl is of nearly no tetragonal distortion and was Al rich in composition, providing a high concentration of antistructure Al atoms on Ti sites.

The temperature of our investigations was very low compared to that of the order-disorder transition of about 1350 K; thus, the defect concentration in the sample is supposed to be very low.[2,23] The possible diffusion mechanisms are then limited to highly correlated mechanisms via one defect, which should have lower activation energies than low correlated mechanisms which do need the activation of more than one defect for atomic migration.[33,34] Lower correlated mechanisms could, of course, dominate at higher temperatures, where the defect concentration increases. The change of mechanism of diffusion with temperature is well known in *B*2 alloys such as CoGa or NiAl (Refs. 34–36) and was also found in $L1_0$-ordered γ-TiAl.[27,37] It is generally accepted for the *B*2 alloys that the proportion of highly correlated mechanisms like the six-jump cycle (6JC) decreases with rising temperature[35] and less correlated mechanisms as the triple defect mechanism or antistructure bridges (ASB) begin to prevail for *B*2 (Refs. 33 and 38) and $L1_0$ alloys.[27,37] In analogy, a low-temperature mechanism for iron diffusion in the *c*-axis direction in FePt with the $L1_0$ structure might be a mechanism corresponding to the *B*2-6JC starting with a vacancy on the Pt lattice.[39] For the high-temperature region lower correlated mechanisms like the ASB mechanism might operate, starting with a vacancy on the Fe lattice. Resistivity measurements and Monte Carlo simulations[27,39,40] indicate that the mechanisms of atomic ordering in intermetallic compounds are very similar to the mechanisms of diffusion and both phenomena operate via the same defect structure.[29] Therefore, we propose that each mechanism might be driven by Fe antisites on the Pt lattice via nearest-neighbor jumps of Fe atoms.

Finally, we want to conclude that we determined the coefficient for iron diffusion in crystalline FePt thin films of $L1_0$ structure in the low-temperature region by means of grazing incidence nuclear-resonant scattering. The method used was successively applied to investigate diffusion in a well-ordered alloy and gives access to very small diffusion lengths.

(i) For successive annealing steps, the decrease of the nuclear multilayer peak intensities was observed. The activation energy and the diffusion constant were determined as $Q=1.65(29)$ eV and $D_0=3.45(44)\times10^{-13}$ m^2 s^{-1}.

(ii) The results of nuclear resonant scattering are in agreement with residual resistivity data of order-order relaxations.

(iii) Deviation from the results of radio-tracer data for the high-temperature region may be explained by the change of the diffusion mechanism with temperature.

(iv) We therefore propose that the mechanisms of order-order relaxation and mass transport diffusion are the same for FePt thin films.

(v) We suggest that the diffusion mechanisms at the low-temperature region is a highly correlated mechanism similar to the $B2$-6JC, and at the high-temperature region a low-correlated mechanism similar to the $B2$-ASB mechanism, respectively.

Compared to other NRS experiments,[9,10] determining directly elementary jump processes, the method presented in this paper gives no information about elementary jump processes or direct access to jump models. Jump models have to be revealed indirectly in combination with other methods. We finally stress that the method presented in this paper has great power in studying diffusion on nanoscale systems. The diffusion coefficients accessible for investigation can be *tuned* by choosing the temperature for the successive annealing steps. To avoid too fast or slow mixing of the layer structure, i.e., the decrease of the nuclear Bragg peaks, the annealing time can be adjusted appropriately. This gives unique access to very low diffusion coefficients. The technique is particularly appropriate to study thin-film layers of metals and alloys. It can be applied to alloys that are difficult to obtain as bulk single crystals, but may be grown as thin films. The same holds for metastable systems.

ACKNOWLEDGMENTS

We thank the European Synchrotron Radiation Facility for provision of synchrotron radiation facilities. We kindly acknowledge the financial support from the Austrian Fonds zur Förderung der wissenschaftlichen Forschung Contract No. FWF P-15421, bm:bwk Contract No. GZ 45.529/2-VI/B/7a/2002 (MDN) and the 6th framework program of the European Union Contract No. 001516 (DYNASYNC). The work at Leuven was supported by the Concerted Action of the K.U. Leuven (Grant No. GOA/2004/02), the University Attraction Pole Grant No. IUAP P5/1, and the Centers of Excellence Programme Grant No. INPAC EF/05/005. We kindly thank B. Laenens and N. Planckaert (K.U. Leuven) for the characterization of the isotopic multilayer. We thank G. Langer (University of Debrecen) for the analysis of the isotopic layer structure of the multilayer.

*Also at ESRF, BP 220, 38043 Grenoble, France.

[1] Y. Nosé, T. Ikeda, H. Nakajima, and H. Numakura, Defect Diffus. Forum **237-240**, 450 (2005).
[2] A. Kushida, K. Tanaka, and H. Numakura, Mater. Trans., JIM **44**, 34 (2003).
[3] R. Kozubski, M. Kozlowski, K. Zapala, V. Pierron-Bohnes, W. Pfeiler, M. Rennhofer, B. Sepiol, and G. Vogl, J. Phase Equilib. **26**, 482 (2005).
[4] A. Gupta, M. Gupta, S. Chakravarty, R. Ruffer, and H. C. Wille, and O. Leupold, Phys. Rev. B **72**, 014207 (2005).
[5] R. Rüffer and A. Chumakov, Hyperfine Interact. **97/98**, 589 (1996).
[6] A. Chumakov, L. Niesen, D. Nagy, and E. Alp, Hyperfine Interact. **123/124**, 427 (1999).
[7] D. Kmiec, B. Sepiol, M. Sladecek, G. Vogl, J. Korecki, and T. Slezak, Defect Diffus. Forum **237-240**, 1222 (2005).
[8] H. Mehrer, in *Diffusion in Condensed Matter*, edited by P. Heitjans and J. Kärger (Springer, New York, 2005), p. 3.
[9] B. Sepiol, A. Meyer, G. Vogl, R. Rüffer, A. Chumakov, and A. Baron, Phys. Rev. Lett. **76**, 3220 (1996).
[10] G. Vogl and B. Sepiol, in *Diffusion in Condensed Matter*, edited by P. Heitjans and J. Kärger (Springer, New York, 2005), p. 65.
[11] J. DuMond and J. Youtz, J. Appl. Phys. **11**, 375 (1940).
[12] H. Cook and J. Hilliard, J. Appl. Phys. **40**, 2191 (1969).
[13] M. Gupta, A. Gupta, J. Stahn, M. Horisberger, T. Gutberlet, and P. Allenspach, Phys. Rev. B **70**, 184206 (2004).
[14] W. H. Wang, H. Y. Bai, M. Zhang, J. H. Zhao, X. Y. Zhang, and W. K. Wang, Phys. Rev. B **59**, 10811 (1999).
[15] H. Bracht, S. Nicols, W. Walukiewicz, J. Silveira, F. Briones, and E. Haller, Nature (London) **408**, 69 (2000).
[16] H. D. Fuchs, W. Walukiewicz, E. E. Haller, W. Dondl, R. Schorer, G. Abstreiter, A. Rudnev, A. Tikhomirov, and V. Ozhogin, Phys. Rev. B **51**, 16817 (1995).
[17] Y. Takahashi, K. Hono, T. Shima, and K. Takanashi, J. Magn. Magn. Mater. **267**, 248 (2003).
[18] J. Staunton, S. Ostanin, S. Razee, B. Gyorffy, L. Szunyogh, B. Ginatempo, and E. Bruno, J. Phys.: Condens. Matter **16**, 5623 (2004).
[19] G. H. O. Daalderop, P. J. Kelly, and M. F. H. Schuurmans, Phys. Rev. B **44**, 12054 (1991).
[20] M. Kim and S. Shin, J. Appl. Phys. **90**, 2211 (2001).
[21] Y. Endo, N. Kikuchi, O. Kitakami, and Y. Shimada, J. Appl. Phys. **89**, 7065 (2001).
[22] M. Hong, K. Hono, and M. Watanabe, J. Appl. Phys. **84**, 4403 (1998).
[23] H. Kudielka and P. Runow, Z. Metallkd. **67**, 699 (1976).
[24] M. Kim, S. Shin, and K. Kang, Appl. Phys. Lett. **80**, 3802 (2002).
[25] A. Cebollada, D. Weller, J. Sticht, G. R. Harp, R. F. C. Farrow, R. F. Marks, R. Savoy, and J. C. Scott, Phys. Rev. B **50**, 3419

(1994).
[26] S. Kroll, H. Mehrer, N. Stolwijk, C. Herzig, R. Rosenkranz, and G. Frommeyer, Z. Metallkd. **83**, 591 (1992).
[27] C. Herzig and S. Divinski, Intermetallics **12**, 993 (2004).
[28] M. Salamon and H. Mehrer, Philos. Mag. A **79**, 2137 (1999).
[29] R. Kozubski, M. Kozlowski, V. Pierron-Bohnes, and W. Pfeiler, Z. Metallkd. **95**, 880 (2004).
[30] C. Lee, R. Nakamura, T. Shimozaki, and T. Okino, Defect Diffus. Forum **237-240**, 426 (2005).
[31] M. Sladecek, B. Sepiol, D. Kmiec, J. Korecki, T. Slezak, and G. Vogl, Defect Diffus. Forum **237-240**, 1225 (2005).
[32] T. Ikeda, H. Kadowaki, and H. Nakajima, Acta Mater. **49**, 3475 (2003).
[33] H. Mehrer, M. Eggersmann, A. Gude, M. Salamon, and B. Sepiol, Mater. Sci. Eng., A **239–240**, 889 (1997).
[34] N. Stolwijk, M. Van-Gend, and H. Bakker, Philos. Mag. A **42**, 783 (1980).
[35] S. Divinski and C. Herzig, Intermetallics **8**, 1357 (2000).
[36] M. Rennhofer, B. Sepiol, W. Loeser, and G. Vogl, Intermetallics **11**, 573 (2003).
[37] S. Divinski, F. Hisher, C. Klinkenberg, and C. Herzig, Intermetallics **14**, 792 (2006).
[38] I. Belova and G. Murch, Intermetallics **6**, 115 (1998).
[39] P. Oramus, M. Kozlowski, R. Kozubski, V. Pierron-Bohnes, M. Cadeville, and W. Pfeiler, Mater. Sci. Eng., A **365**, 166 (2004).
[40] R. Kozubski, S. Czekaj, M. Kozlowski, E. Partyka, and K. Zapala, J. Alloys Compd. **378**, 302 (2004).